Solvent Dependent Conformation of a Regioselective Amylose Carbamate. Amylose-2-acetyl-3,6-bis(phenylcarbamate)

Maiko Tsuda,[1] Ken Terao,[1] Shinichi Kitamura,[2] Takahiro Sato[1]

[1] *Department of Macromolecular Science, Graduate School of Science, Osaka University, 1-1 Machikaneyama-cho, Toyonaka, Osaka 560-0043, Japan*
[2] *Graduate School of Life and Environmental Sciences, Osaka Prefecture University, Gakuen-cho, Nakaku, Sakai, Osaka 599-8531, Japan*

Correspondence to: Ken Terao; email: kterao@chem.sci.osaka-u.ac.jp

Contact grant sponsor: Japan Society for the Promotion of Science (JSPS)
Contact grant number: 23750128
Contact grant sponsor: Japan Synchrotron Radiation Research Institute (JASRI)
Contact grant number: 2007B1296, 2008A1313, and 2009A1049

ABSTRACT:

Six amylose-2-acetyl-3,6-bis(phenylcarbamate) (AAPC) samples ranging in weight-average molar mass M_w *from* 1.8×10^4 *to* 1.1×10^6 *have been prepared from enzymatically synthesized amylose samples. Static light scattering, small-angle X-ray scattering, sedimentation equilibrium, and viscosity measurements were made for the samples in 1,4-dioxane (DIOX), 2-ethoxyethanol (2EE), and 2-butanone (MEK) all at 25 °C to determine particle scattering functions, z-average radii of gyration, intrinsic viscosities as well as* M_w*. The data were analyzed in terms of the wormlike cylinder model mainly to yield the helix pitch per residue* h *and the Kuhn segment length* λ^{-1}*, which corresponds to twice of the persistence length. The latter parameters* (λ^{-1}) *in 2EE (11 nm) and MEK (12 nm) are quite smaller than those for amylose tris(phenylcarbamate) (ATPC) in the same solvent (16 nm in 2EE and 18 nm in MEK) whereas those for AAPC (21 nm) and ATPC (22 nm) in DIOX are essentially the same as each other. This indicates that the chain stiffness of AAPC is more strongly influenced by the solvents since the number of intramolecular H-bonds of AAPC is more changeable than that for ATPC.*

Keywords: Polysaccharide derivative; hydrogen bond; chain stiffness

INTRODUCTION

Interaction among the neighbor units in a polymer chain or between the polymer and solvent molecules determines the local and global conformation of the polymer chain in solution. For example, specific conformations of biopolymers[1] (fibrous proteins, nucleic acids, and polysaccharides) or some synthetic foldamers[2,3] are influenced by intra- and inter-molecular hydrogen bonds. Dimensional and hydrodynamic properties of a polymer in a solvent is still hardly to be predicted precisely only from their chemical structures whereas these properties for almost all linear polymers can be modeled by the Kratky-Porod (KP) wormlike chain[4] (or more generally, the helical wormlike chain[5,6]), in which polymer chains are characterized by the stiffness parameter λ^{-1} (Kuhn segment length, which is equal to twice of the persistence length) and the helix pitch per residue h (a parameter of the local chain length). Systematical work to determine these parameters for well-defined polymers in various solvents is thus still desired. Linear polysaccharide derivatives may be suitable to investigate the relationship because some derivatives are easily prepared from native polysaccharides and furthermore their main chain has almost perfect stereoregularity compared with vinyl polymers.

In those polymers, we have recently paid attention to amylose carbamates since the amylosic main chain has helical nature and both λ^{-1} and h may be influenced by hydrogen bonding of carbamate groups. Indeed, amylose and its derivatives have various h values from 0.10 to 0.40 nm in the crystal structure.[7,8,9] Dilute solution properties have been thus studied for amylose tris(phenylcarbamate) (ATPC) and amylose tris(*n*-butylcarbamate) (ATBC), for which the chemical structures are illustrated in Figure 1. We found that both λ^{-1} and h significantly depend on the side group and solvents, and furthermore, the intramolecular hydrogen bond (H-bond) between C=O and NH groups plays an important role in the high chain stiffness.[10,11,12] As seen from infrared adsorption, about 50% polar groups are, however, still free in tetrahydrofuran (THF) and 1,4-dioxane (DIOX) even when the polymer has high stiffness, suggesting that such residual polar sites do not contribute to

the chain stiffness. Therefore, regioselective carbamate derivatives having fewer carbamate groups may be helpful to understand the relationship between chain stiffness and number of polar groups on a glucosidic unit. However, few studies have been reported on conformational properties of regioselective amylose carbamates in solution.

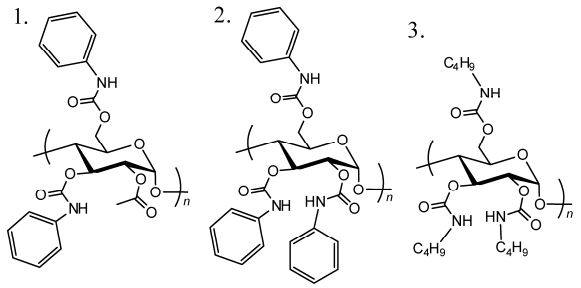

FIGURE 1 Chemical structures of (1) AAPC, (2) ATPC, and (3) ATBC.

Recently, Dicke [13] reported quantitative synthesis of 2-acetylamylose under a mild condition. This allowed us to obtain some regioselective derivatives of amylose. We therefore synthesized a regioselective amylose bis(phenylcarbamate), that is, amylose-2-acetyl-3,6-bis(phenylcarbamate) (AAPC, **1** in Figure 1), which has two phenylcarbamate groups on C-3 and C-6 position and a small acetyl group on C-2 group. We made light and small-angle X-ray scattering (SAXS), viscosity measurements on AAPC in DIOX, 2-ethoxyethanol (2EE), and in 2-butanone (MEK) and furthermore circular dichroism and infrared absorption measurements in the former two solvents. The obtained molecular parameters are compared with those for ATPC how the number of H-bonding sites are affectable to the chain stiffness.

EXPERIMENTAL

Samples and Solvents

AAPC samples were synthesized from an excess amount of phenylisocyanate and 2-acetylamylose, which had been prepared from six enzymatically synthesized amylose

samples[14] for which the weight-average molar mass M_w ranges from 6×10^3 to 5×10^5 and the dispersity index (the ratio of M_w to the number-average molar mass M_n) is less than 1.2. A procedure to prepare an AAPC sample is as follows. It should be noted that similar regioselective derivatives have been synthesized by Kondo et al.[15]

Synthesis of 2-acetylamylose.[13] An amylose sample (3.0 g) dissolved into dehydrated DMSO (40 – 60 mL) in a reaction vessel at 80 °C. Vinyl acetate (4 mL) and Na_2HPO_4 (60 mg) as a catalyst were added into the resultant solution at room temperature and then it was stirred at 40 °C for 70 hours. After the catalyst was removed by centrifuge, the supernatant was added to a large amount of 2-propanol to precipitate 2-acetylamylose, which was dried in a vacuum oven at 60 – 80 °C. Yield: 4 – 9 g.

Synthesis of AAPC. A dried 2-acetylamylose sample was dissolved into dry pyridine including lithium chloride (ca. 7 g). An excess amount of phenylisocyanate (three times of OH groups of 2-acetylamylose) was added and stirred at 80 – 100 °C for 12 – 15 hours. The reaction mixture was poured into a large amount of methanol to precipitate AAPC. Each AAPC sample was further purified by successive fractional precipitation with acetone or THF as solvents and methanol as a precipitant to remove impurities including unreacted isocyanate. Appropriate middle fractions from respective AAPC samples were reprecipitated from THF to methanol and dried in vacuum. The obtained six samples were designated as AAPC1100K, AAPC500K, AAPC200K, AAPC100K, AAPC50K, and AAPC20K based on the molar mass. Mass ratio of carbon to nitrogen for each sample measured by elemental analysis was consistent with the calculated value from the chemical structure within ±3%, indicating that C-3 and C-6 positions were fully substituted by phenylcarbamate groups. The chemical structure was also confirmed by ^{1}H-NMR in acetone-d_6 as well as solid-state IR spectra. The dispersity index (M_w/M_n) was estimated to be between 1.02 and 1.11 by using

the size exclusion chromatography equipped with a multi-angle lager light scattering: both M_w and M_n were determined from the scattering intensity and concentration (by refractive index detector) at each elution volume. DMSO (dehydrate grade), Na_2HPO_4, and vinyl acetate were used without further purification. Lithium chloride was dried in vacuum at 90°C for 2 hours. Pyridine, DIOX, 2EE, and MEK were purified by fractional distillation over CaH_2.

Static Light Scattering (SLS)

SLS measurements were made on a Fica-50 light scattering photometer for AAPC1100K, AAPC500K, AAPC200K, and AAPC100K in DIOX, 2EE, and MEK, and for AAPC50K in DIOX all at 25 °C. Five solutions with different polymer mass concentrations c were measured. Procedures including optically clean and calibration of the photometer were described in ref 10. Vertically polarized incident light of 436 nm wavelength was used and the reduced scattering intensities $R_{\theta,Hv}$ and $R_{\theta,Uv}$ was measured with or without analyzer in the horizontal direction, respectively, in a scattering angle θ ranging from 22.5° to 150°. Optically anisotropic effects were not negligible for AAPC50K, AAPC100K, and AAPC200K as is the case of amylose tris(3,5-dimethylphenylcarbamate) (ADMPC)[16] and cellulose tris(3,5-dimethylphenylcarbamate) (CDMPC).[17] Indeed, the optical anisotropy factor δ was at most 1.00×10^{-2}, which causes 7 % error to M_w from $R_{\theta,UV}$. Based on the current theories for light scattering data with the anisotropic effects,[18,19,20] the following equations were used to determine δ, M_w, the second virial coefficient A_2, and an apparent radius of gyration $\langle S^2 \rangle^*$, which is related to the z-average mean square radius of gyration $\langle S^2 \rangle_z$ (see RESULTS AND DISCUSSION).

$$\lim_{c\to 0}\left(\frac{Kc}{R_{\theta,\mathrm{Uv}}}\right)^{1/2} = M_{\mathrm{w,app}}^{-1/2} P(q)_{\mathrm{app}}^{-1/2} = M_{\mathrm{w,app}}^{-1/2}\left[1+\frac{1}{6}\left\langle S^2\right\rangle_{\mathrm{z,app}}^{1/2} q^2 + \ldots\right] \qquad (1)$$

$$\lim_{\theta\to 0}\left(\frac{Kc}{R_{\theta,\mathrm{Uv}}}\right)^{1/2}=\left(\frac{Kc}{R_{0,\mathrm{Uv}}}\right)^{1/2}=M_{\mathrm{w,app}}^{-1/2}\left[1+A_{2,\mathrm{app}}M_{\mathrm{w,app}}c+\ldots\right] \tag{2}$$

$$\lim_{c\to 0}\frac{R_{0,\mathrm{Hv}}}{R_{0,\mathrm{Uv}}}=\frac{3\delta}{1+7\delta} \tag{3}$$

where

$$M_{\mathrm{w,app}}=(1+7\delta)M_{\mathrm{w}} \tag{4}$$

$$\left\langle S^2\right\rangle_{\mathrm{z,app}}=(1+7\delta)^{-1}\left\langle S^2\right\rangle^{*} \tag{5}$$

$$A_{2,\mathrm{app}}=(1+7\delta)^{-2}A_2 \tag{6}$$

Here, K and q are the optical constant and the magnitude of the scattering vector. The obtained M_w's in the different solvents are consistent within ±4% for AAPC500K and AAPC200K but those for AAPC1100K and AAPC100K in 2EE were ~20% larger than those for the corresponding sample in DIOX and MEK, hence the data for the two samples in 2EE were not further analyzed in this paper. The values of A_2 were $3 - 5 \times 10^{-4}$ mol g^{-2}cm^3 in DIOX, $\sim 1 \times 10^{-4}$ mol g^{-2}cm^3 in MEK, and $\sim 0.4 \times 10^{-4}$ mol g^{-2}cm^3 in 2EE, indicating that these are good solvents for AAPC at 25 °C. The specific refractive index increments $\partial n/\partial c$ for AAPC samples were determined to be 0.142 cm^{3}g^{-1}, 0.179 cm^{3}g^{-1}, and 0.152 cm^{3}g^{-1} in DIOX, MEK, and 2EE, respectively, all at 436 nm wavelength at 25 °C.

Ultracentrifugation

Sedimentation equilibrium measurements were made for AAPC20K in DIOX at 25 °C by using a Beckman Optima XL-I ultracentrifuge at a rotor speed of 25,000 rpm to determine M_w, the z-average molar mass M_z, and A_2 since we do not have enough amount to determine M_w by light scattering. See refs 10 and 21 for experimental details and data analysis,

respectively. The partial specific volume and $\partial n/\partial c$ at the used wavelength (675 nm) were determined to be 0.715 cm^3g^{-1} and 0.125 cm^3g^{-1}, respectively, for AAPC in DIOX at 25 °C. The latter value is 12% smaller than that at the wavelength used for light scattering (436 nm). Similar wavelength dependence was also found for other polymer solvent systems[22] including amylose carbamate derivatives.[10,11,12,16]

Small-Angle X-Ray Scattering (SAXS)

SAXS measurements were carried out for AAPC50K and AAPC20K in DIOX, MEK, and 2EE at 25 °C at the BL40B2 beamline in SPring-8 (see ref 10 for experimental details) since the radii of gyration of the samples are too small to be determined by SLS. The camera length and the wavelength were set to be 1500 mm and 0.1 nm, respectively. The particle scattering function $P(q)$ and $\langle S^2 \rangle_z$ were determined from the excess scattering intensities for four solutions with different c in terms of the Berry square-root plot.[18]

Viscometry

Solvent and solution viscosities for the six AAPC samples in DIOX, MEK, and 2EE at 25 °C were measured using an Ubbelohde type viscometer. The specific viscosity was evaluated by taking into account the difference between the solution and solvent densities. The obtained Huggins constant ranges between 0.3 and 0.9 for the five larger M_w samples and the maximum value is 1.5 for AAPC20K in MEK and 2EE.

Infrared Absorption (IR), Circular Dichroism (CD), and DFT calculations

IR and CD measurements were made for AAPC in DIOX and 2EE at 25 °C on an FT/IR-4200 (JASCO) with a solution cell made of CaF_2 and having 0.05 mm path length and a J720WO spectropolarimeter (JASCO) with a rectangular quartz cell having 1 mm path length. The polymer mass concentration was adjusted to 1.5×10^{-2} g cm^{-3} for IR and 8×10^{-5} g cm^{-3}

for CD. The calculations based on the density functional theory were performed using the Gaussian 03 program.[23] Methyl acetate (MEA) was chosen as a model compound for the acetyl group of AAPC and methylphenylcarbamate (MPC) for the phenylcarbamate group. The conformation was optimized using the B3LYP/6-311+G(d,p) level theory with a scaling factor of 0.9679.[24] The absorption band corresponding to the hydrogen bonding C=O stretching band was calculated when an NH group of a MPC molecule or an OH group of methanol (MeOH) molecule is placed nearby the C=O group.

RESULTS AND DISCUSSION

Dimensional and Hydrodynamic Properties

Figure 2 illustrates q^2 dependence of $P(q)^{-1/2}$ (or $P(q)_{app}^{-1/2}$ from SLS) for AAPC samples in DIOX, MEK, and 2EE at 25 °C. The gyration radius $\langle S^2 \rangle_z$ from SAXS and $\langle S^2 \rangle_{app}$ from SLS were determined as initial slopes and the former values are summarized in Table I along with the intrinsic viscosities $[\eta]$ and the average M_w from different solvents. The molar mass dependence of $[\eta]M_0$ is displayed in Figure 3 along with those for ATPC in the corresponding solvents, [10,16] where M_0 denotes the molar mass of the repeat unit. The $[\eta]M_0$ data for the polymers in DIOX are almost equivalent in the investigated range of molar mass, indicating the almost the same main-chain conformation. On the other hand, those for AAPC in MEK and 2EE are significantly smaller than that in DIOX for the same sample whereas those for ATPC in MEK and 2EE are only slightly smaller than those in DIOX. These indicate that AAPC has semiflexible backbone but dimensions of the main chain are more affectable by the solvent than those for ATPC. This conformational feature was also seen in the $P(q)$ data. The Holtzer plots[25] [$qP(q)$ vs q] in Figure 4 are typical for the wormlike chain with finite thickness. The peak at $q \sim 0.2$ nm^{-1} for AAPC50K in MEK and 2EE are appreciably larger than that in DIOX, indicating less chain stiffness in MEK and 2EE comparing to that in DIOX.

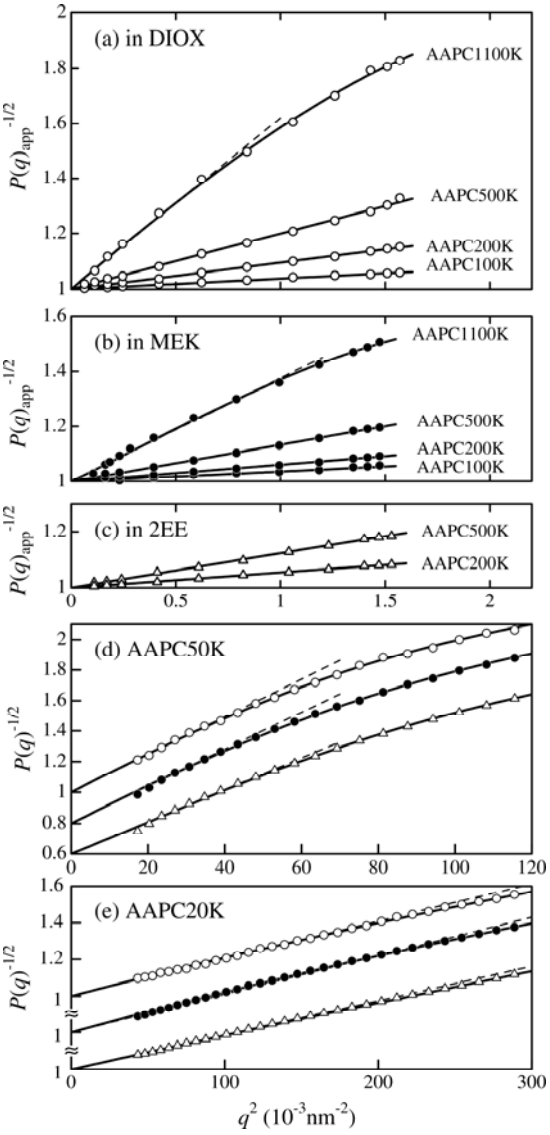

FIGURE 2 Angular dependence of $P(q)_{app}^{-1/2}$ [from SLS, (a), (b), and (c)] and $P(q)^{-1/2}$ [from SAXS, (d) and (e)] for indicated AAPC samples in DIOX (unfilled circles), MEK (filled circles), and 2EE (triangles) all at 25 °C.

Table I Molecular Characteristics and Physical Properties of AAPC Samples in 1,4-Dioxane (DIOX), 2-Butanone (MEK), and 2-Ethoxyethanol (2EE) at 25 °C

Sample	$M_w/10^4$ (g mol^{-1})	in DIOX		in MEK		in 2EE	
		$\langle S^2\rangle_z^{1/2}$ (nm)	$[\eta]$ (cm^{3}g^{-1})	$\langle S^2\rangle_z^{1/2}$ (nm)	$[\eta]$ (cm^{3}g^{-1})	$\langle S^2\rangle_z^{1/2}$ (nm)	$[\eta]$ (cm^{3}g^{-1})
AAPC1100K	108 [a]	61.0 [a]	312	47.5 [a]	173		139
AAPC500K	48.4 [a]	34.6 [a]	221	28.3 [a]	128	27.1 [a]	110
AAPC200K	23.0 [a]	24.2 ± 0.3 [a]	122	19.3 ± 0.2 [a]	70.3	18.0 ± 0.2 [a]	66.2
AAPC100K	11.1 [a]	15.3 ± 0.4 [a]	60.5	14.9 ± 0.2 [a]	45.3		40.8
AAPC50K	5.43 [a]	8.6 [b]	30.7	8.5 [b]	26.6	7.9 [b]	24.0
AAPC20K	1.79 [c]	3.50 [b]	14.1	3.55 [b]	12.0	3.35 [b]	10.7

[a] SLS.

[b] SAXS.

[c] Sedimentation equilibrium.

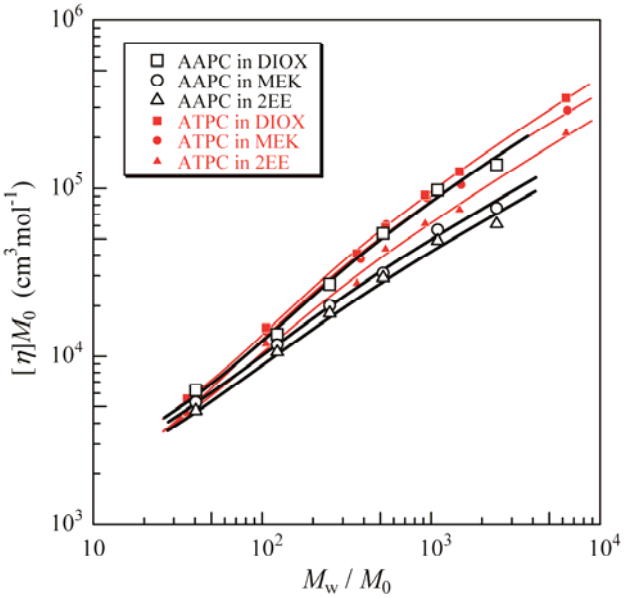

FIGURE 3 Molar mass dependence of $[\eta]M_0$ for AAPC in DIOX (unfilled squares), MEK (unfilled circles), 2EE (unfilled triangles) along with our previous data [10,16] for ATPC in DIOX (filled squares), MEK (filled circles), and 2EE (filled triangles), all at 25 °C. Solid curves, theoretical values for the wormlike cylinder model with the parameters listed in Table III.

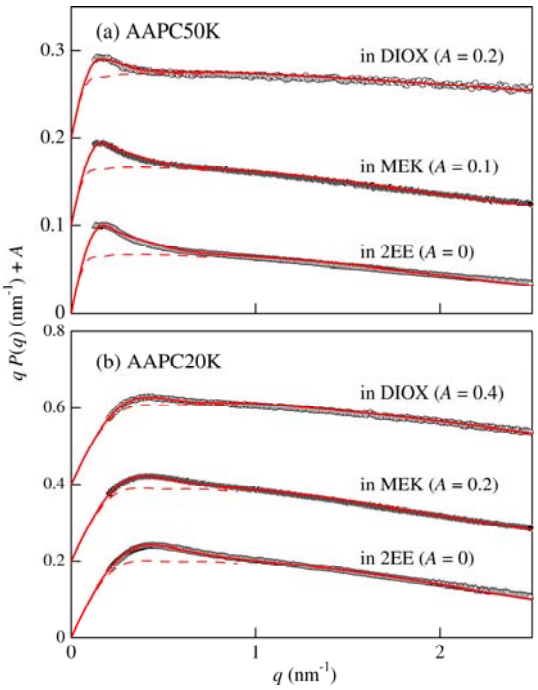

FIGURE 4 Holtzer plots from SAXS for (a) AAPC50K and (b) AAPC20K in DIOX (unfilled circles), in MEK (filled circles), and in 2EE (triangles) all at 25 °C. The ordinate values are shifted by A for clarity. Solid and dashed curves represent theoretical values for the unperturbed wormlike cylinder with the parameters in Table III and those in the rod limit ($\lambda^{-1} = \infty$), respectively.

Intramolecular H-bonding and Helical Structure

As mentioned in our previous papers, intramolecular H-bonds stiffen and keep the locally helical structure of the main chain of amylose carbamates.[10,11,12] These H-bonds can be observed as split amide I band in solution IR spectra. Figure 5 shows the molar absorption coefficient ε vs wavenumber for AAPC100K in DIOX and 2EE at 25 °C along with those for ATPC. Two peaks at 1759 cm^{-1} and 1704 cm^{-1} are substantially the same as those observed for ATPC (at 1754 cm^{-1} and 1706 cm^{-1}), corresponding to the free and intramolecular H-bonding C=O groups, respectively.[10] Since the calculated absorption band for free (or H-bonding) acetyl and carbamate groups (see Table II) are quite close to each other, the degree of intramolecular H-bonding of AAPC in the two solvents may be estimated from the peak

heights in the IR spectra. The latter peak at 1704 cm^{-1} is appreciably lower in 2EE than in DIOX. This should be reflected that a larger number of intramolecular H-bonding C=O groups in DIOX than in 2EE. On the contrary, CD spectrum (molar circular dichroism $\Delta\varepsilon$ vs the wavelength λ_0 in vacuum) for AAPC in DIOX is substantially the same as that in 2EE (Figure 6), suggesting that the local helical structure in the two solvents are similar with each other. Furthermore, the former peak at 1759 cm^{-1} in 2EE is appreciably smaller and the gap between the two peaks is shallower than that in DIOX as is the case with ATPC. This is likely due to the increase in the degree of intermolecular H-bonding between C=O group of AAPC and OH group of 2EE (Figure 5).

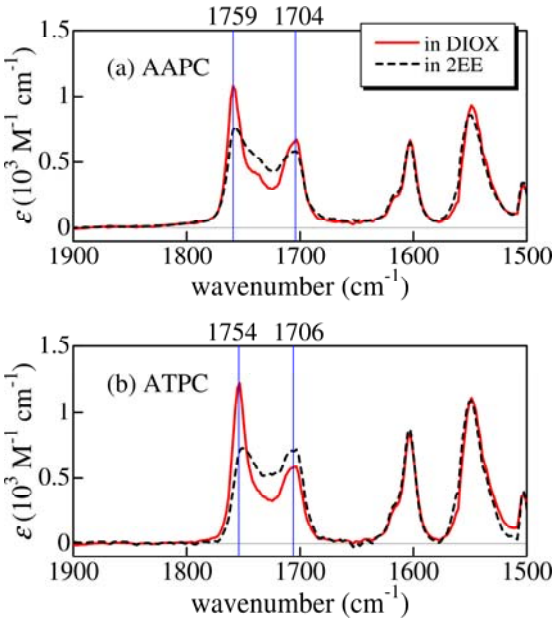

FIGURE 5 IR spectra for (a) AAPC100K and (b) ATPC300K [10] in DIOX (solid curve) and in 2EE (dashed curve) at 25 °C.

Table II Calculated IR Wavenumbers for C=O Stretching Band of AAPC Side Groups and in the Presence of MPC and MeOH

System	Interaction	*wavenumber* (cm^{-1})
MEA	Free	1739
MEA+MPC	C=O…H-N	1725
MEA+MeOH	C=O…H-O	1714
MPC	Free	1733
MPC+MPC	C=O…H-N	1716
MPC+MeOH	C=O…H-O	1718

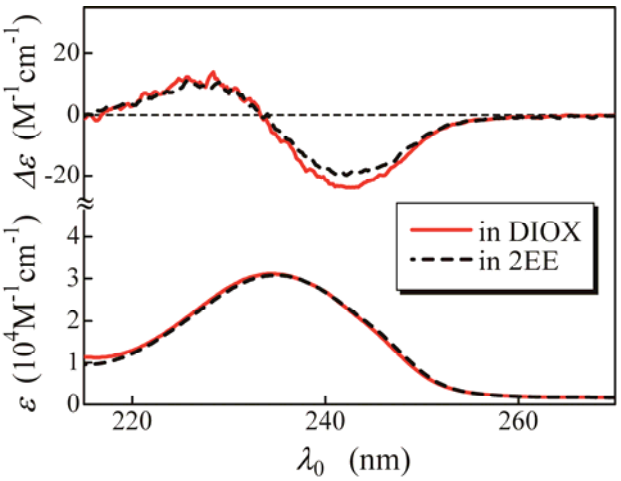

FIGURE 6 CD and UV spectra for AAPC20K in DIOX (solid curve) and in 2EE (dashed curve) at 25 °C.

Wormlike Chain Analysis

The Holtzer plots in Figure 4 were analyzed in terms of the Nakamura-Norisuye theory[26] for the wormlike cylinder. The molar mass per unit contour length M_L, λ^{-1}, and the chain diameter d characterize the model. Since the experimental $qP(q)$'s have appreciable peaks at low q region and they cannot be explained by the theoretical rod-limiting values (dashed curves), the three parameters are unequivocally determined from the curve fitting procedure and listed in Table III. Theoretical $qP(q)$ values calculated from the three parameters reproduce the experimental values almost quantitatively.

Table III Wormlike Chain Parameters for AAPC in DIOX, MEK, and 2EE at 25 °C Determined by Three Different Methods from $P(q)$, $[\eta]$, and $\langle S^2 \rangle_z$

Method	M_L (nm^{-1})	λ^{-1} (nm)	d (nm)
in DIOX			
$P(q)$	1340 ± 30	21 ± 2	1.1 ± 0.1
$[\eta]$	1340 [a]	19.5 ± 3	2.9 ± 0.3
$\langle S^2 \rangle_z$	1300 ± 50	23 ± 2	–
in MEK			
$P(q)$	1230 ± 30	14 ± 3	1.65 ± 0.1
$[\eta]$	1230 [a]	10.5 ± 2	2.5 ± 0.3
$\langle S^2 \rangle_z$	1200 ± 50	14 ± 3	–
in 2EE			
$P(q)$	1270 ± 50	12 ± 3	1.55 ± 0.1
$[\eta]$	1270 [a]	9.5 ± 2	2.4 ± 0.3
$\langle S^2 \rangle_z$	1260 ± 50	12 ± 5	–

[a] Assumed values.

Viscosity data are also analyzed by the wormlike cylinder model for which $[\eta]$ is formulated by Yamakawa and coworkers.[5,27,28] Since the excluded-volume effect to $[\eta]$ might not be negligible for high M_w region, it was taken into account by the quasi-two-parameter scheme[5,29,30] combined with the Barrett function.[31] Therefore theoretical $[\eta]$ is characterized by M_L, λ^{-1}, and d, and the excluded volume strength. Assuming the M_L value from $P(q)$, λ^{-1} and d are determined as listed in Table III and the excluded volume effects were negligible in the M_w range investigated. The obtained λ^{-1} in each solvent is fairly consistent with that from $P(q)$ whereas the d value from $[\eta]$ is much larger than those from $P(q)$. This inconsistency is well known for amylose carbamates[10,11,12,16,32,33] as well as for the other polymers[5,34,35] because the d value from $[\eta]$ reflects the hydrodynamic friction while that from $P(q)$ is determined from the electron density profile including side groups and solvent molecules around the chain contour.

Now, let us consider the optical anisotropic effects on the radius of gyration $\langle S^2 \rangle$. Assuming cylindrically symmetric polarizabilities of the main chain, $\langle S^2 \rangle^*$ in the Nagai scheme[36] is expressed in a good approximation as[37]

$$\left\langle S^2 \right\rangle^* = \left\langle S^2 \right\rangle - f\left(\lambda, L, \varepsilon\right) \tag{7}$$

where ε is the polarizability parameter and related to δ which is obtained from SLS measurements using eq 3.

$$\delta = \frac{\varepsilon^2 M_{\mathrm{L}}}{135\lambda M}\left\{1 - \frac{M_{\mathrm{L}}}{6\lambda M}\left[1 - \exp\left(-\frac{6\lambda M}{M_{\mathrm{L}}}\right)\right]\right\} \tag{8}$$

The theoretical δ values calculated using the λ^{-1} and M_{L} values in Table III and $|\varepsilon| = 1.9$ fairly fit the experimental data as shown in Figure 7. This $|\varepsilon|$ is the same order as those for CDMPC ($|\varepsilon| = 2.8$)[17] and ADMPC ($|\varepsilon| = 0.5 - 1.2$).[16] The second term of the right hand side in eq 7 is much smaller than $\langle S^2 \rangle^*$, that is at most ± 2.6 %. Since the sign of ε cannot be determined from SLS, we showed this small term as an error in the column for $\langle S^2 \rangle_z$ in Table I. The obtained $\langle S^2 \rangle_z$ data plotted against M_{w} in Figure 8 are analyzed by using the Benoit-Doty equation[38] for the unperturbed wormlike chain

$$\left\langle S^2 \right\rangle = \frac{L}{6\lambda} - \frac{1}{4\lambda^2} + \frac{1}{4\lambda^3 L} - \frac{1}{8\lambda^4 L^2}\left[1 - \exp\left(-2\lambda L\right)\right] \tag{9}$$

since both the intramolecular excluded volume effects and chain thickness are negligible in the M_{w} range investigated; the latter was estimated as an addition of $d^2/8$ to the right hand

side in eq 9 [39] with the d value determined from $P(q)$. The two parameters, M_L and λ^{-1}, are therefore unequivocally determined from the curve fitting procedure and listed in Table III; they are substantially the same as those determined from $P(q)$ and $[\eta]$, showing the wormlike chain is a good model for this polymer in the three solvents. The average parameters from the three methods are summarized in Table IV. The obtained h values of AAPC are in a rather narrow range between 0.34 and 0.36 nm which are fairly close to the crystal structure of amylose esters (0.37 – 0.40 nm)[9,40] and double helical amylose (0.35 nm),[7,41] thus they should be reasonable.

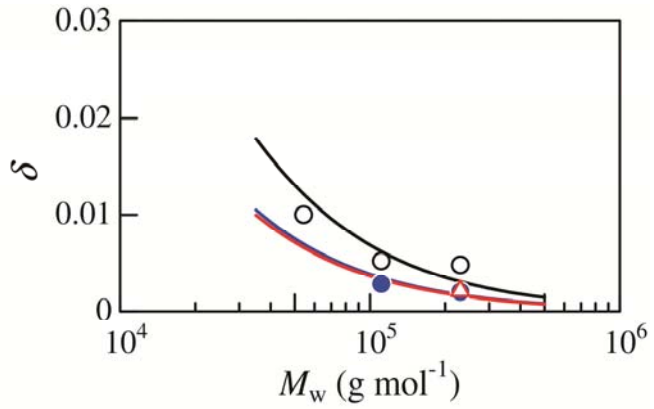

FIGURE 7 Molar mass dependence of the optical anisotropy factor δ for AAPC in DIOX (unfilled circles), MEK (filled circles), and MEA (triangles) at 25 °C. Curves represent the theoretical values calculated from eq 8 (see text for the parameters).

Table IV Values of the Helix Pitch per Residue *h* and the Kuhn Segment Length λ^{-1} for AAPC and ATPC in DIOX, MEK, and 2EE at 25 °C

Polymer	Solvent	h (nm)	λ^{-1} (nm)
AAPC	DIOX	0.34 ± 0.01	21 ± 2
	MEK	0.36 ± 0.02	12 ± 2
	2EE	0.35 ± 0.02	11 ± 2
ATPC	DIOX [a]	0.34 ± 0.01	22 ± 2
	MEK [b]	0.39 ± 0.02	18 ± 2
	2EE [a]	0.32 ± 0.01	16 ± 2

[a] Ref. 10.

[b] Ref. 16.

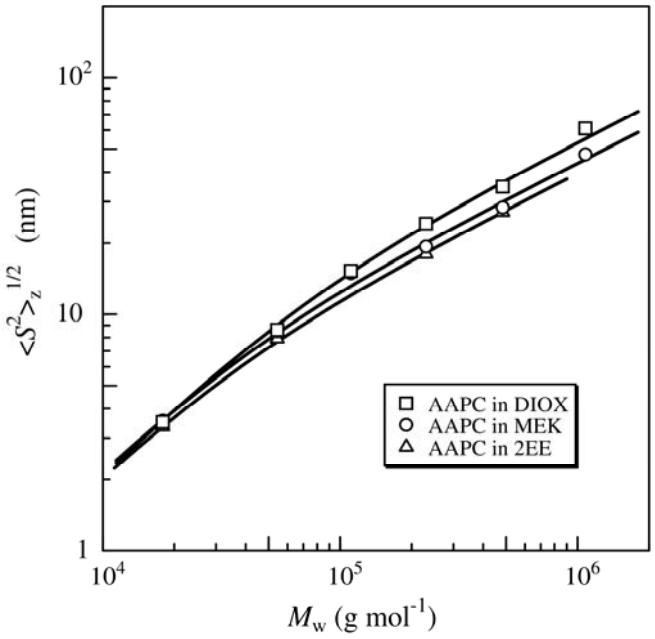

FIGURE 8 Molar mass dependence of $<S^2>_z^{1/2}$ for AAPC in DIOX (squares), MEK (circles), and 2EE (triangles) all at 25 °C. Solid curves, theoretical values for the wormlike chain model with the parameters in Table III.

Comparison between AAPC and ATPC

Table IV includes our previous wormlike chain parameters for ATPC.[10,16] In DIOX, both the two parameters as well as the IR spectra of the amide I band for AAPC are almost the same as those for ATPC, indicating that the difference in the substituent at the C-2 position does not cause an appreciable difference to the local and global conformation in the solvent. On the other hand, in higher polar solvents, that is 2EE and MEK, the chain stiffness λ^{-1} of AAPC is appreciably lower than those for ATPC. This suggests that the intramolecular H-bonds in AAPC are easier to be broken by polar solvents than in ATPC probably owing to the less bulkiness of side groups of AAPC and/or less numbers of NH group in each repeat unit of AAPC. Indeed, the degree of intramolecular H-bonding C=O groups for AAPC in 2EE obtained by IR is appreciably smaller than that in DIOX whereas the difference in the two solvents is hardly distinguishable for ATPC.[10]

CONCLUSIONS

The Kuhn segment length λ^{-1} and helix pitch per residue h were determined for AAPC (**1** in Figure 1) in DIOX, 2EE, and MEK. The latter parameter is in a narrow range between 0.34 and 0.36 nm, which is close to that for crystal structure of amylose esters. Though the chain stiffness in DIOX is as high as that for ATPC in the same solvents, those in 2EE and MEK are quite smaller than those for ATPC in the corresponding solvents, indicating that polar solvents may break the intramolecular H-bonds more easily than that for ATPC owing to the less bulkiness of side groups.

REFERENCES

1. Alberts, B.; Johnson, A.; Lewis, J.; Raff, M.; Roberts. K.; Walter, P. Molecular biology of the cell, 4th ed; Garland Science: New York, 2002.
2. Gellman, S. H. Acc Chem Res 1998, 31, 173-180.
3. Hill, D. J.; Mio, M. J.; Prince, R. B.; Hughes, T. S.; Moore, J. S. Chem Rev 2001, 101, 3893-4011.
4. Kratky, O.; Porod, G.; Recl Trav Chim Pays-Bas 1949, 68, 1106-1122.
5. Yamakawa, H. Helical wormlike chains in polymer solutions; Springer: Berlin, 1997.
6. Yamakawa, H. Polym J 1999, 31, 109-119.
7. Popov, D.; Buléon, A.; Burghammer, H.; Chanzy, N.; Montesanti, N.; Putaux, J.-L.; Potocki-Veronese, G.; Riekel, C. Macroolecules 2009, 42, 1167-1174.
8. Cardoso, M. B.; Putaux, J.-L.; Nishiyama, Y.; Helbert, W.; Hytch, M.; Silveira, N. P.; Chanzy, H. Biomacromolecules 2007, 8, 1319-1326.
9. Zugenmaier, P.; Steinmeier, H. Polymer 1986, 27, 1601-1608.
10. Terao, K.; Fujii, T.; Tsuda, M.; Kitamura, S.; Norisuye, T. Polym J 2009, 41, 201-207.

11. Terao, K.; Murashima, M.; Sano, Y.; Arakawa, S.; Kitamura, S.; Norisuye, T. Macromolecules 2010, 43, 1061-1068.

12. Sano, Y.; Terao, K.; Arakawa, S.; Ohtoh, M.; Kitamura, S.; Norisuye, T. Polymer 2010, 51, 4243-4248.

13. Dicke, R. Cellulose 2004, 11, 255-263.

14. Kitamura, S.; Yunokawa, H.; Mitsuie, S.; Kuge, T. Polym J 1982, 14, 93-99.

15. Kondo, S.; Yamamoto, C.; Kamigaito, M.; Okamoto, Y. Chem Lett 2008, 37, 558-559.

16. Tsuda, M.; Terao, K.; Nakamura, Y.; Kita, Y.; Kitamura, S.; Sato, T. Macromolecules 2010, 43, 5779-5784.

17. Tsuboi, A.; Norisuye, T.; Teramoto, A. Macromolecules 1996, 29, 3597-3602.

18. Berry G. C. J Chem Phys 1966, 44, 4550-4564.

19. Yamakawa, H. Modern Theory of Polymer Solutions; Harper & Row: New York, 1971.

20. Nagai, K. Polym J 1972, 3, 67-83.

21. Norisuye, T.; Yanaki, T.; Fujita, H. J Polym Sci Polym Phys Ed 1980, 18, 547-558.

22. Huglin, M. B. Light scattering from polymer solutions; Academic Press: London, 1972.

23. Frisch, M. J.; Trucks, G. W.; Schlegel, H. B.; Scuseria, G. E.; Robb, M. A.; Cheeseman, J. R.; Montgomery, Jr., J. A.; Vreven, T.; Kudin, K. N.; Burant, J. C.; Millam, J. M.; Iyengar, S. S.; Tomasi, J.; Barone, V.; Mennucci, B.; Cossi, M.; Scalmani, G.; Rega, N.; Petersson, G. A.; Nakatsuji, H.; Hada, M.; Ehara, M.; Toyota, K.; Fukuda, R.; Hasegawa, J.; Ishida, M.; Nakajima, T.; Honda, Y.; Kitao, O.; Nakai, H.; Klene, M.; Li, X.; Knox, J. E.; Hratchian, H. P.; Cross, J. B.; Bakken, V.; Adamo, C.; Jaramillo, J.; Gomperts, R.; Stratmann, R. E.; Yazyev, O.; Austin, A. J.; Cammi, R.; Pomelli, C.; Ochterski, J. W.; Ayala, P. Y.; Morokuma, K.; Voth, G. A.; Salvador, P.; Dannenberg, J. J.; Zakrzewski, V. G.; Dapprich, S.; Daniels, A. D.; Strain, M. C.; Farkas, O.; Malick, D. K.; Rabuck, A. D.; Raghavachari, K.; Foresman, J. B.; Ortiz, J. V.; Cui, Q.; Baboul, A. G.; Clifford, S.; Cioslowski, J.; Stefanov, B. B.; Liu, G.; Liashenko, A.; Piskorz, P.; Komaromi, I.; Martin, R. L.; Fox, D. J.; Keith, T.; Al-Laham, M. A.; Peng, C. Y.; Nanayakkara, A.;

Challacombe, M.; Gill, P. M. W.; Johnson, B.; Chen, W.; Wong, M. W.; Gonzalez, C.; Pople, J. A. Gaussian 03, Rev. E.01; Gaussian, Inc., Wallingford, CT, 2004.

24. Andersson, M. P.; Uvdal, P. J Phys Chem A 2005, 109, 2937-2941.

25. Holtzer, A. J. J Polym Sci 1955, 17, 432-434.

26. Nakamura, Y.; Norisuye, T. J Polym Sci Part B Polym Phys 2004, 42, 1398-1407.

27. Yamakawa, H.; Fujii, M. Macromolecules 1974, 7, 128-135.

28. Yamakawa, H.; Yoshizaki, T. Macromolecules 1980, 13, 633-643.

29. Yamakawa, H.; Stockmayer, W. H. J Chem Phys 1972, 57, 2843-54.

30. Shimada, J.; Yamakawa, H. J Chem Phys 1986, 85, 591-599.

31. Barrett, A. J.; Macromolecules 1984, 17, 1566-1572.

32. Fujii, T.; Terao, K.; Tsuda, M.; Kitamura, S.; Norisuye, T. Biopolymers 2009, 91, 729-736.

33. Arakawa, S.; Terao, K.; Kitamura, S.; Sato, T. Polym Chem 2012, 3, 472-478.

34. Hickl, P.; Ballauff, M.; Scherf, U.; Mullen, K.; Lindner, P. Macromolecules 1997, 30, 273-279.

35. Terao, K.; Mizuno, K.; Murashima, M.; Kita, Y.; Hongo, C.; Okuyama, K.; Norisuye, T.; Bächinger, H. P.; Macromolecules 2008, 41, 7203-7210.

36. Nagai, K. Polym J 1972, 3, 67-83.

37. Sakurai, K.; Ochi, K.; Norisuye, T.; Fujita, H. Polym J 1984, 16, 559-567.

38. Benoit, H.; Doty, P. J Phys Chem 1953, 57, 958-963.

39. Konishi, T.; Yoshizaki, T.; Saito, T.; Einaga, Y.; Yamakawa, H. Macromolecules 1990, 23, 290-297.

40. Takahashi, Y.; Nishikawa, S. Macromolecules 2003, 36, 8656-8661.

41. Takahashi, Y.; Kumano, T.; Nishikawa, S. Macromolecules 2004, 37, 6827-6832.